Journal of Physics: Conference Series

PAPER • OPEN ACCESS

Prediction of dynamic response of semi-submersible floating offshore wind turbines by a novel hydrodynamic coefficient model

To cite this article: Yuliang Liu and Takeshi Ishihara 2019 *J. Phys.: Conf. Ser.* **1356** 012035

Prediction of dynamic response of semi-submersible floating offshore wind turbines by a novel hydrodynamic coefficient model

Yuliang Liu[1] **and Takeshi Ishihara**[1]

[1] Department of Civil Engineering, School of Engineering, The University of Tokyo, Japan,7-3-1 Hongo, Bunkyo, 113-8656 Tokyo, Japan

E-mail: ishihara@bridge.t.u-tokyo.ac.jp

Abstract. A novel hydrodynamic coefficients model is proposed for the components of floating offshore wind turbine (FOWT). First, the formulas for evaluation of the added mass and drag coefficient for the components of FOWT are proposed to consider the interaction effects between columns as well as the frequency and amplitude dependencies. The global matrices of hydrodynamic coefficients are then evaluated by the proposed formulas and validated by the experimental data from the forced oscillation test. The predicted dynamic response of FOWT is also validated by the water tank test. Finally, the improvement of dynamic behaviour of the platform by the skirts is investigated. The decrease of amplitude and the increase of natural period for the heave motion of the platform with skirts are successfully simulated by the proposed model.

1. Introduction

In recent years, diversified types of floating platform have been applied in floating offshore wind turbines (FOWTs) and studied through experiments and numerical simulations. In Hywind project [1], the world's first spar type FOWT was positioned in Norway. Three FOWTs with different types of platform were built off the coast of Fukushima in Japan [2]. The first one is a 2MW semi-submersible FOWT and the others are a 5MW advanced spar FOWT and a 7MW V-shape semi-submersible FOWT. In addition, a 3 MW FOWT was installed by IDEOL in 2018 [3]. These platforms consist of several type of components, as such, circular and rectangular cylinders as well as heave plates which are used to improve the performance of FOWT. In order to accurately evaluate the motions of FOWTs, the hydrodynamic coefficients of these components in various ocean conditions are necessary. The water tank test is a general method to obtain hydrodynamic coefficients of platforms oscillating in different amplitudes and periods, however it needs a lot of costs due to manufacture of models and arrangement of tests. Computational fluid dynamics (CFD) is another powerful tool for prediction of hydrodynamic coefficients, which can provide accurate distribution of pressure. However, the numerical simulation by CFD is time consuming if fine grids are used and a large number of simulations are required.

It is well known that added mass and drag coefficients, which represent hydrodynamic inertia force and viscous drag force acting on the offshore structure [4], are two critical coefficients for prediction of hydrodynamic loading. These coefficients for an isolated cylinder depend on Reynolds number (Re), Keulegan–Carpenter number (KC) and surface roughness [5]. To discuss the effect of frequency of oscillation on the hydrodynamic coefficients, the frequency parameter β is also used for oscillating flows. It is defined as the ratio of Reynolds number to KC number.

For a complex floating structure, such as a semi-submersible type of FOWT, the interaction between columns affects the hydrodynamic force on each column [6], especially when the columns are arranged closely between each other. The hydrodynamic coefficients of cylinders are commonly decided by the experimental data. However, a cylinder in the complex floating structure may interfere with flow field around another cylinder, which leads to variation of hydrodynamic coefficients. In OC4, added mass and drag coefficients of three upper columns in DeepCwind semi-submersible platform were defined as the same value based on the experiment of a single circular cylinder [7]. Benitz et al. [6] conducted CFD simulations for the same platform to evaluate drag coefficients of each column in the current condition with a constant velocity. They pointed out that the effect of interaction between the multi-columns changes the drag coefficients greatly and it should be included in prediction of hydrodynamic loading. Liang and Tao [8] demonstrated that the drag coefficient of rear column was smaller than that of frontal ones. The influence of distance between cylinders on hydrodynamic forces was studied experimentally at a constant Reynolds number using four cylinders with equal diameters arranged in the in-line square configuration [9]. The flow pattern and hydrodynamic coefficients were found to be strongly dependent on the distance between cylinders.

Numerous investigations have been dedicated to establishing dependency of KC, β and Re on added mass and drag coefficients. Sarpkaya [10] measured the hydrodynamic coefficients of two dimensional cylinders in the oscillating flow and found that drag coefficients decreased while added mass coefficients increased as β increases. Both of them approached a constant value when Reynolds number become quite high. Zhang and Ishihara [11] studied the added mass and drag coefficients of heave plates for an advanced spar platform through the forced oscillation test by CFD. The formulas to predict hydrodynamic coefficients of heave plate considering effect of KC number, thickness and diameter were proposed. A series of forced oscillation tests of a large-scale heave plate used in a semi-submersible FOWT were carried out by Carlos and Iglesias [12] for investigating variation of hydrodynamic coefficients in different amplitudes and frequencies. Both added mass and drag coefficients of heave plate were dominated by KC. Kamizawa et al. [13] compared the designed value with observed motion response of an advanced spar platform in Fukushima FORWARD [2]. It was found that the predicted sway motion was overestimated since a constant drag coefficient was applied.

In this study, a novel hydrodynamic coefficients model for various components of FOWT is described in section 2. The effect of interaction between cylinders of FOWT is evaluated based on the numerical simulations by CFD, and Re, β and KC dependencies are investigated based on previous studies for single cylinder. In section 3, the proposed model is validated by the global matrices of hydrodynamic coefficients from the forced oscillation test. The effect of skirts on the dynamic response of the semi-submersible platform is investigated by the proposed model and validated by the water tank test. Finally, the conclusions are given in section 4.

2. Hydrodynamic coefficient models

A 1:50 scale model of 2MW FOWT is firstly described in section 2.1. The hydrodynamic coefficients for each component of the platform is then defined in section 2.2. The correction factor representing the effect of interaction of columns is introduced in section 2.3. Finally, influences of β and KC on the hydrodynamic coefficients are investigated in section 2.4.

2.1. Model description

A 1:50 scale model of 2MW FOWT used in Fukushima FORWARD [2] is used for study of hydrodynamic coefficients. As shown in Fig. 1, the platform comprises a central column linked with base of the tower and three side columns that are connected to the central one through three pontoons and braces. At the base of side column, three heave plates are set to shift natural period of heave out range of wave energy and suppress motion of the platform in wave. Three heave plates and the central column are connected by three rectangular pontoons with variable cross sections.

IOP Conf. Series: Journal of Physics: Conf. Series **1356** (2019) 012035 doi:10.1088/1742-6596/1356/1/012035

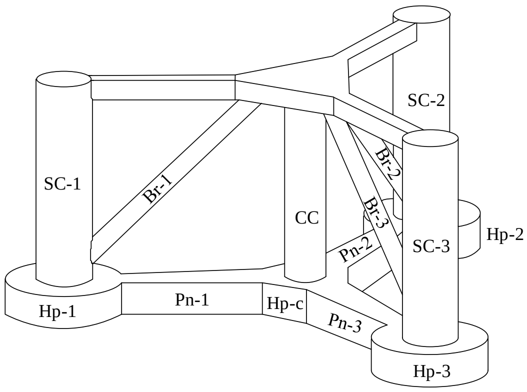

(a) Bird view of the platform

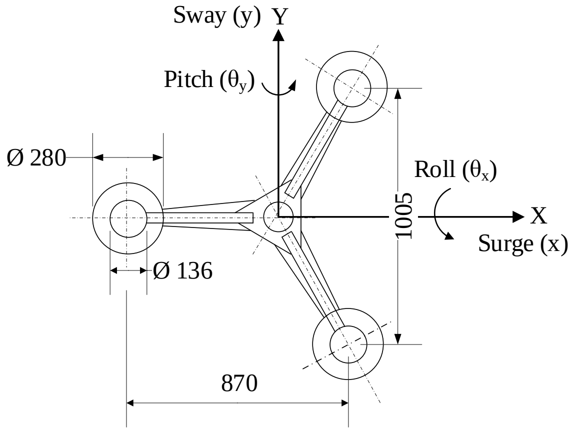

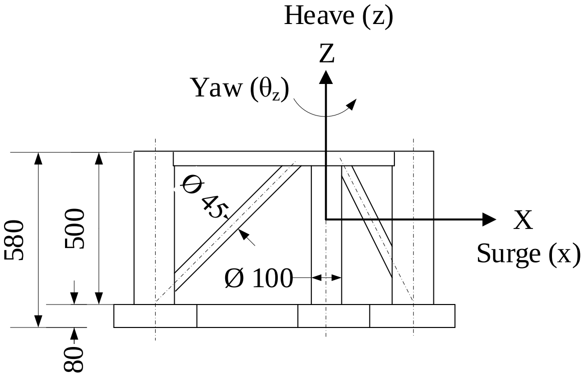

(b) Top view of the platform (Unit: mm)

(c) Side view of the platform (Unit: mm)

Figure. 1. Configuration of 1:50 scale model of the semi-submersible platform for a 2MW FOWT

Table 1. Dimension and hydrostatic properties of the semi-submersible platform

Elements	Dimension (m)
Draft of the platform	0.38
Elevation of center column (CC) and side columns (SC) above SWL	0.2
Spacing between side columns	1.005
Height of center column and side columns	0.5
Diameter of center column	0.1
Diameter of side columns	0.136
Depth to top of heave plate (Hp) below SWL	0.3
Height of heave plate and pontoon (Pn)	0.08
Diameter of heave plate	0.28
Width of pontoon	0.06~0.12
Length of pontoon	0.39
Diameter of brace (Br)	0.045
Height of deck	0.045
Width of deck	0.045
Center of gravity below SWL	-0.166
Meta-centric height above SWL	0.086
Radius of gyration K_{xx}	0.41
Radius of gyration K_{yy}	0.41

Origin of the coordinate is defined at the gravity center as presented in Fig.1. The degrees of freedom (DOFs) for the platform involve translational surge, sway and heave motions and rotational roll, pitch and yaw motions.

A summary of Dimension and hydrostatic properties of the platform is described in Table. 1. Displaced water of the platform is 42.2kg including contribution from mooring lines.

2.2. Definition of hydrodynamic coefficients for each component of the platform

The Morison's equation and the boundary element method (BEM) are widely used for assessing the hydrodynamic loads on the FOWT [14], [15]. BEM provides linear wave induced force and motion induced force. However, viscous drag force on structure resulting from flow separation cannot be predicted by BEM because of the basic assumption of inviscid flow. Morison's equation is an empirical formula to calculate inertial and viscous drag forces on the slender structure. The KC dependent added mass and drag coefficients of isolated cylinder obtained from the previous study are used. The frequency-dependent radiation damping force in the time domain is calculated by Cummins equation.

The equation of motion for a FOWT in waves [15] is written as follows:

$$[\mathbf{M}]\{\ddot{\mathbf{x}}\}+[\mathbf{C}]\{\dot{\mathbf{x}}\}+[\mathbf{K}]\{\mathbf{x}\}=\{\mathbf{F}_G\}+\{\mathbf{F}_B\}+\{\mathbf{F}_H\}+\{\mathbf{F}_M\}+\{\mathbf{F}_R\} \tag{1}$$

where $\mathbf{M}$, $\mathbf{C}$ and $\mathbf{K}$ are mass, damping and stiffness matrices of the platform respectively. $\{\mathbf{x}\}$, $\dot{\mathbf{x}}$ and $\ddot{\mathbf{x}}$ represent displacement, velocity and acceleration vector of the platform at a specified reference point. $\{\mathbf{F}_G\}$, $\{\mathbf{F}_B\}$, $\{\mathbf{F}_H\}$, $\{\mathbf{F}_M\}$ and $\{\mathbf{F}_R\}$ denote the gravitational, buoyancy, hydrodynamic, mooring line and restoring forces, respectively. The restoring force is calculated by the matrix of hydrostatic stiffness [16] as follows:

$$\mathbf{F}_R=[K_R]\{x\} \tag{2}$$

$$K_R=\begin{bmatrix} 0 & 0 & 0 & 0 & 0 & 0 \\ 0 & 0 & 0 & 0 & 0 & 0 \\ 0 & 0 & -\rho_w g A_w & 0 & 0 & 0 \\ 0 & 0 & 0 & -W\times GM_X & 0 & 0 \\ 0 & 0 & 0 & 0 & -W\times GM_Y & 0 \\ 0 & 0 & 0 & 0 & 0 & 0 \end{bmatrix} \tag{3}$$

where W is the weight of the platform and A_w is the area of water plane. GM_X and GM_Y represent the meta-centric heights of the platform about x and y axes respectively.

The hydrodynamic force can be written as sum of hydrodynamic inertia force, linear radiation damping, incident wave excitation and fluid viscous effect as shown in Eq. (4). Higher order hydrodynamic force is not considered in this study.

$$\mathbf{F}_H=\mathbf{F}_{m,a}+\mathbf{F}_{m,d}+\mathbf{F}_{w,F-K}+\mathbf{F}_{w,d}+\mathbf{F}_{drag} \tag{4}$$

where $\mathbf{F}_{m,a}$ and $\mathbf{F}_{m,d}$ are the hydrodynamic inertia and linear radiation damping forces, $\mathbf{F}_{w,F-K}$ and $\mathbf{F}_{w,d}$ indicate the Froude-Krylov (F-K) and diffraction forces, $\mathbf{F}_{drag}$ is the viscous drag force that is proportional to square of relative velocity. $\mathbf{F}_{m,a}$ and $\mathbf{F}_{drag}$ are classified as the motion induced forces due to the movement of platform and $\mathbf{F}_{m,d}$, $\mathbf{F}_{w,F-K}$ and $\mathbf{F}_{w,d}$ are treated as wave induced forces. The hydrodynamic inertia and drag forces of a cylinder in the local coordinate are estimated by equations as:

$${}_iF^n_{m,a}={}_iC^n_a\rho\forall_i\ddot{x}_i \qquad {}_iF^n_{drag}=\frac{1}{2}\rho\,{}_iC^n_d A^n_i(u^n_i-\dot{x}^n_i)\left|u^n_i-\dot{x}^n_i\right| \tag{5}$$

where ${}_iC_a^n$ and ${}_iC_d^n$ are the added mass and drag coefficients of the cylinder in the normal direction, ρ and $\forall_i$ indicate the density of water and the displaced volume of water, $u_i^n - \dot{x}_i^n$ represents the relative velocity of the cylinder to water particle, A_i^n is the project area of the cylinder in the normal direction. Both ${}_iC_a^n$ and ${}_iC_d^n$ are dependent on β and KC .

KC expresses the relative amplitude of fluid oscillation to characteristic length and is defined as:

$$KC=\frac{uT}{L}=\frac{2\pi a}{L} \tag{6}$$

where u and T are the amplitude of velocity and period of oscillation. In a sinusoidal oscillation, uT can be presented by $2\pi a$ where a is the amplitude of motion. The characteristic length L of the semi-submersible platform is the diameter of side column for the horizontal movement and the diameter of side heave plate for the vertical oscillation.

Re is the ratio of inertia force to viscous force and defined as:

$$Re=\frac{\rho uL}{\mu}=\frac{uL}{\upsilon}=\frac{2\pi aL}{T\upsilon} \tag{7}$$

where μ and υ are the dynamic and kinematic viscosities of fluid. In sinusoidal oscillation, u indicates the amplitude of velocity of object relative to fluid, thus Re relates the amplitude and period of oscillation at the same time. In the oscillation flow, the frequency parameter β is widely used and expressed by the ratio of Reynolds number to KC number as:

$$\beta=\frac{Re}{KC}=\frac{D^2}{\upsilon T}=\frac{\omega D^2}{2\pi\upsilon} \tag{8}$$

BEM offers the added mass coefficients with the assumption that the motion of the platform is small and can perform well at low KC . However, the added mass coefficients C_a at high KC may be different from those at low KC due to the nonlinearity of fluid. The drag coefficient C_d varies greatly with β and KC and plays an important role on the motion of the platform near the resonance period. In this study, β and KC are used as independent variables and Re is calculated by the product of β and KC .

The added mass and drag coefficients of a cylinder can be determined by β , KC , the surface roughness k_s and the correction factor of interaction effect η . The effect of surface roughness on the hydrodynamic coefficients is not discussed in this study since the surface of model in the water tank tests is smooth. The hydrodynamic coefficients for each component of the platform can be expressed as a function of β , KC and η :

$${}_iC_a^k(\beta^k,KC^k,\eta^k)={}_rC_a^k(\beta_0^k,KC_0^k)\times{}_r\gamma_a^k\times{}_i\eta_a^k \tag{9}$$

$${}_iC_d^k(\beta^k,KC^k,\eta^k)={}_rC_d^k(\beta_0^k,KC_0^k)\times{}_r\gamma_d^k\times{}_i\eta_d^k \tag{10}$$

where subscript i indicates the component i of the platform and superscript k represents the direction of hydrodynamic coefficients, which expresses the normal direction by n or the axial direction by t. ${}_iC_a^k(\beta^k,KC^k,\eta^k)$ and ${}_iC_d^k(\beta^k,KC^k,\eta^k)$ express the added mass and drag coefficients of the component i at β^k and KC^k with consideration of the correction factor of interaction effect η^k in the k direction. ${}_rC_a^k(\beta_0^k,KC_0^k)$ and ${}_rC_d^k(\beta_0^k,KC_0^k)$ indicate the representative C_a and C_d for the referenced component r at β_0^k and KC_0^k in the k direction. ${}_i\eta_a^k$ and ${}_i\eta_d^k$ are the correction factors for interaction effect on the component i in the k direction, ${}_r\gamma_a^k$ and ${}_r\gamma_d^k$ are the correction factors for frequency and amplitude effects on the referenced component r in the k direction.

The correction factors ${}_i\eta_a^k$ and ${}_i\eta_d^k$ are defined as the ratio between the hydrodynamic coefficients of the component i and the referenced component r as shown in Eq. (11):

$$ {}_{i}\eta_{a}^{k} = \frac{{}_{i}C_{a}^{k}(\beta^{k}, KC^{k})}{{}_{r}C_{a}^{k}(\beta^{k}, KC^{k})} \qquad {}_{i}\eta_{d}^{k} = \frac{{}_{i}C_{d}^{k}(\beta^{k}, KC^{k})}{{}_{r}C_{d}^{k}(\beta^{k}, KC^{k})} \tag{11} $$

where ${}_{i}C_{a}^{k}(\beta^{k}, KC^{k})$ and ${}_{i}C_{d}^{k}(\mathrm{Re}^{k}, KC^{k})$ are the added mass and drag coefficients of component i at β^{k} and KC^{k} in the k direction. The components, such as SC-2, Hp-2 without the interaction effect are chosen as the referenced components.

In addition, the correction factors considering the frequency and amplitude effects are defined as:

$$ {}_{r}\gamma_{a}^{k} = \frac{{}_{r}C_{a}^{k}(\beta^{k}, KC^{k})}{{}_{r}C_{a}^{k}(\beta_{0}^{k}, KC_{0}^{k})} \qquad {}_{r}\gamma_{d}^{k} = \frac{{}_{r}C_{d}^{k}(\beta^{k}, KC^{k})}{{}_{r}C_{d}^{k}(\beta_{0}^{k}, KC_{0}^{k})} \tag{12} $$

where ${}_{r}\gamma_{a}^{k}$ and ${}_{r}\gamma_{d}^{k}$ are the correction factors for frequency and amplitude effects on the referenced component r in the k direction.

2.3. Correction factor for interaction effects

During the periodical motion of the platform, the motion of the component disturbs the flow filed and subsequently changes the hydrodynamic loading on other components, especially when the components are close to each other. CFD can consider the interaction effects on the added mass and drag coefficients of components. In this study, the predicted added mass and drag coefficients of components by CFD as shown in Pan and Ishihara [17] is used to investigate the interaction effect between the columns of the platform.

Table 2. Hydrodynamic coefficients of each component at β_0 and KC_0

Components	${}_{i}C_{a}^{n}$	${}_{i}\eta_{a}^{n}$	${}_{i}C_{d}^{n}$	${}_{i}\eta_{d}^{n}$	${}_{i}C_{a}^{t}$	${}_{i}\eta_{a}^{t}$	${}_{i}C_{d}^{t}$	${}_{i}\eta_{d}^{t}$
Side column SC-1	0.88	0.83	0.53	0.60	0	0	0	0
Side column SC-2 *	1.06	1.00	0.95	1.00	0	0	0	0
Side column SC-3	1.06	1.00	0.95	1.00	0	0	0	0
Center column CC	0.90	1.00	1.05	1.00	0	0	0	0
Side heave plate Hp-1	0.37	0.75	0.85	0.60	1.78	1.00	3.09	1.00
Side heave plate Hp-2 *	0.49	1.00	1.43	1.00	1.78	1.00	3.09	1.00
Side heave plate Hp-3	0.49	1.00	1.43	1.00	1.78	1.00	3.09	1.00
Center heave plate Hp-c	0.39	1.00	1.06	1.00	2.10	1.00	3.69	1.00
Pontoon Pn-1-x	1.76	1.00	3.10	1.00	0	0	0	0
Pontoon Pn-2-x*	1.76	1.00	3.10	1.00	0	0	0	0
Pontoon Pn-3-x	1.76	1.00	3.10	1.00	0	0	0	0
Pontoon Pn-1-z	1.82	1.00	3.22	1.00	0	0	0	0
Pontoon Pn-2-z*	1.82	1.00	3.22	1.00	0	0	0	0
Pontoon Pn-3-z	1.82	1.00	3.22	1.00	0	0	0	0
Brace Br-1	0.54	0.34	0.65	0.16	0	0	0	0
Brace Br-2 *	1.36	1.00	1.77	1.00	0	0	0	0
Brace Br-3	1.36	1.00	1.77	1.00	0	0	0	0
Total value	0.73		1.21		1.11		5.55	

The component marked by * is used as the referenced component

Table 2 shows the added mass and drag coefficients of each component at β_{0}^{k} and KC_{0}^{k}, which are 4.72×10^{3} and 4.62 in the surge direction, and are 1.99×10^{4} and 0.9 in the heave direction, respectively. The referenced components are marked by * in Table 2, such as SC-2. Since there are no referenced components for the center column and center heave plate, the interaction correction factors are defined as 1 for them. In Table 2, x and z for the pontoons represent the horizontal and vertical directions because the width of the pontoons in these two directions are different. The total values of hydrodynamic coefficients of the platform in the surge and heave directions are also shown in Table 2.

Fig. 2 displays an example of interaction correction factors of SC-1 for C_a and C_d, which show small variation for different β and KC. For simplicity, the correction factor for interaction effect on each component is set as a constant.

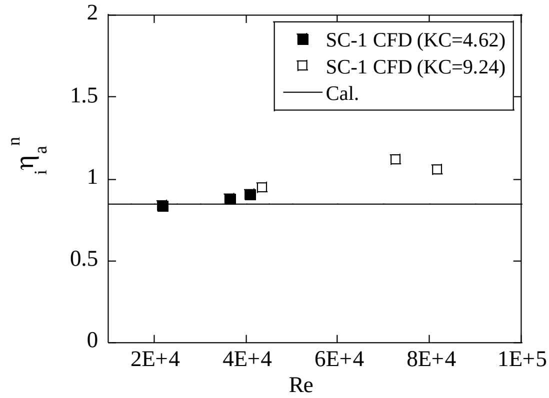

(a) Interaction correction factor for the added mass coefficient

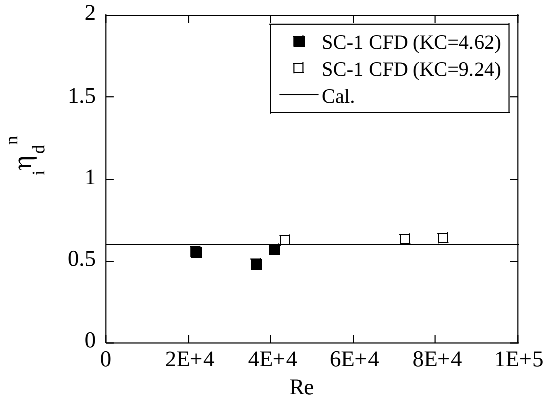

(b) Interaction correction factor for the drag coefficient

Figure 2 . Interaction correction factors for the hydrodynamic coefficients of SC-1

2.4. Correction factor for frequency and amplitude effects

The hydrodynamic coefficients of circular cylinder obtained from CFD simulation by Pan and Ishihara [17] and the previous study [18]are used to predict the correction factors for frequency and amplitude effects on the circular cylinders. For simplicity, the heave plates and columns above them are considered as one component and their correction factors are assumed to be the same. The circular cylinders in the semi-submersible model are classified into 3 types, such as SC, CC, Br, according to different ratio of length to diameter. In this study, the hydrodynamic coefficients of circular cylinders are assumed as a function of Re, which includes the effects of KC and β at the same time. The formulas for the correction factors of each component are presented in Table 3. Ca and Cd of circular cylinders for SC-2 and Br-2 are calculated by the correction factors in Table 3 and reference data in Table 2. As shown in Fig. 3, Ca of the circular cylinder decreases as $\mathrm{Re} = \beta \times KC$ increases and approaches a constant value when Re exceeds a critical value. The lower limit for Cd of the circular cylinder is defined as 0.6, which is the same as the value of two dimensional circular cylinder at high Reynolds number.

For the rectangular cylinder and heave plates, the hydrodynamic coefficients are predicted as a function of KC since they are insensitive to the frequency due to the flow separation. KC for the heave motion is small since the diameter of heave plate is large. In this range, the drag coefficient of heave plate is sensitive to KC, but is insensitive to the frequency. The correction factor for frequency and amplitude effects on the pontoon shown in Table 3 are evaluated based on the experimental data from the forced oscillation test for a square cylinder at KC of 1~14 [18]. The hydrodynamic coefficients obtained from the vertical oscillation test of a circular heave plate is used for the heave plates [19]. The frequency effect on C_a and C_d of heave plate shown in the experiment is relatively small. The hydrodynamic coefficients of heave plates out the range of KC in the experiment is extrapolated by fitting the curve as shown in Fig. 4. C_d of the heave plate decreases rapidly at low KC, while C_a increases slowly. Tables 3 and 4 list the correction factors for each component in the normal and axial directions, respectively. As the axial coefficients of side columns and pontoons are negligible, correction factors of these components are set as 0.

IOP Conf. Series: Journal of Physics: Conf. Series **1356** (2019) 012035 doi:10.1088/1742-6596/1356/1/012035

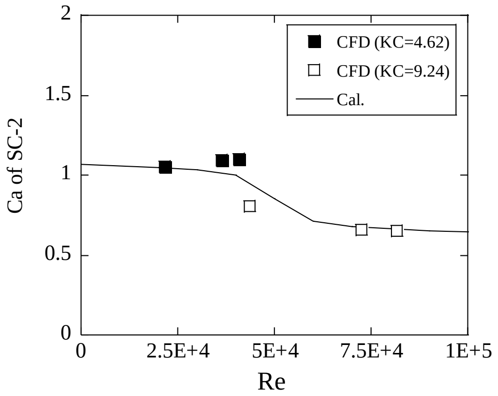

(a) C_a of SC-2

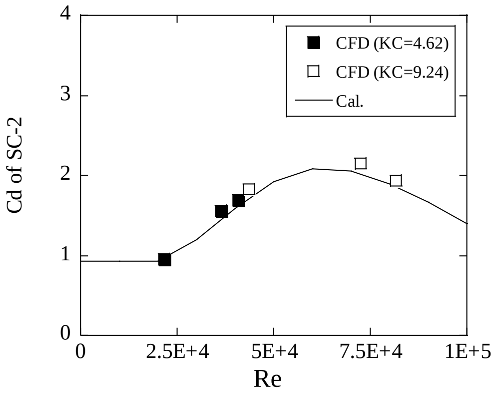

(b) C_d of SC-2

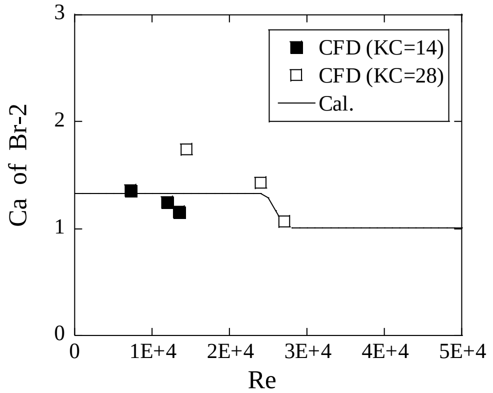

(c) C_a of Br-2

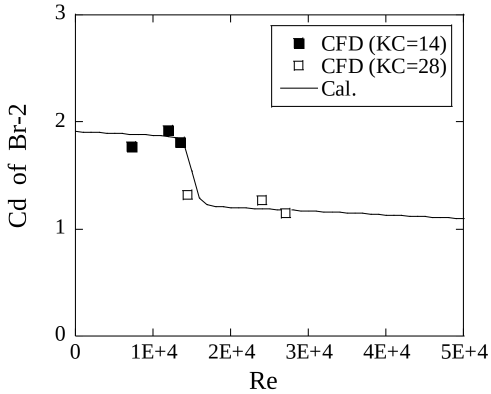

(d) C_d of Br-2

Figure 3. Hydrodynamic coefficients of the circular cylinders in the normal direction.

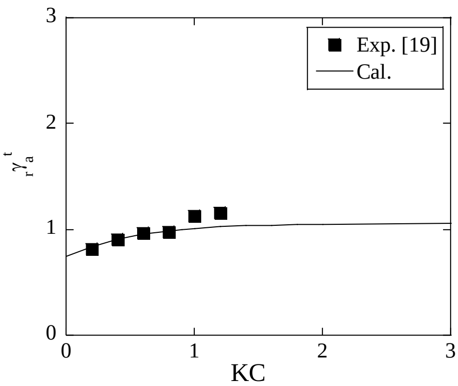

(a) Correction factor for C_a^t of Hp-1

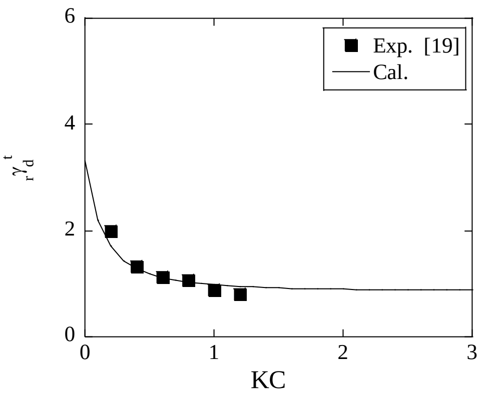

(b) Correction factor for C_d^t of Hp-1

Figure 4. Correction factors of ${}_r\gamma_a^t$ and ${}_r\gamma_d^t$ for the heave plate in the axial direction

Table **3**. Correction factors of frequency and amplitude effects in the normal direction

Component	${}_r\gamma_a^n$ and ${}_r\gamma_d^n$
SC-2, Hp-2 [17]	${}_r\gamma_a^n = \max\left\{-0.15\tanh(1.2\times10^{-5}\times\mathrm{Re}-6)+0.85-10^{-6}\times\mathrm{Re},\ 0.57\right\}$ ${}_r\gamma_d^n = \begin{cases} 0.954 & \mathrm{Re}\le 2\times10^4 \\ \max\left\{1.7\tanh(0.4\times10^{-4}\times\mathrm{Re}-1.52)+2.38-2.6\times(10^{-6}\times\mathrm{Re})^{1.2},\ 0.63\right\} & \mathrm{Re}>2\times10^4 \end{cases}$
CC, Hp-C [17]	${}_r\gamma_a^n = \max\left\{-0.18\tanh(1.2\times10^{-4}\times\mathrm{Re}-6.0)+0.86-10^{-6}\times\mathrm{Re},\ 0.58\right\}$ ${}_r\gamma_d^n = \max\left\{0.4\tanh(4\times10^{-5}\times\mathrm{Re}-0.8)+1.2-4\times(10^{-6}\times\mathrm{Re})^{0.9},\ 0.57\right\}$
Br-2 [17]	${}_r\gamma_a^n = -0.12\tanh(10^{-3}\times\mathrm{Re}-26)+0.86$ ${}_r\gamma_d^n = \max\left\{-0.18\tanh(10^{-3}\times\mathrm{Re}-15)+0.9-5\times10^{-5}\times\mathrm{Re},\ 0.34\right\}$
Pn-2 [18]	${}_r\gamma_a^n = \begin{cases} 0.77 & KC<1.0 \\ 0.34\left(KC+1\right)^{0.3}+0.35 & KC\ge1.0 \end{cases}$ ${}_r\gamma_d^n = -0.45\left(KC+1\right)^{0.33}+1.93$

Table 4. Correction factors of frequency and amplitude effects in the axial direction

Component	${}_r\gamma_a^t$	${}_r\gamma_d^t$
Hp-2 [19]	${}_r\gamma_a^t = 2.26\tanh(KC+1.3)-1.21$	${}_r\gamma_d^t = 0.56(1.5KC+0.44)^{-2.0}+0.83$
Hp-c [19]	${}_r\gamma_a^t = 2.23\tanh(KC+1.3)-1.19$	${}_r\gamma_d^t = 0.58(1.5KC+0.44)^{-2.0}+0.86$
SC-2, CC Pn-2, Br-2	${}_r\gamma_a^t=0$	${}_r\gamma_d^t=0$

3. Validation and application

In order to validate the accuracy of proposed model, the global matrices of hydrodynamic coefficients calculated from the distributed C_a and C_d for each component are compared with those from the forced oscillation tests in section 3.1. The dynamic responses of the platform predicted by the proposed model are then validated by the experimental data from the water tank test in section 3.2. Finally, the effect of skirts on the dynamic responses of the platform is investigated in section 3.3

3.1. Global matrices of hydrodynamic coefficients

The hydrodynamic coefficients of the platform are studied by the forced oscillation test as shown in Fig. 5. The model is sinusoidally oscillated in still water by an actuator connected at the top of the platform. The hydrodynamic coefficients of the platform are calculated by the measured forces. To evaluate hydrodynamic coefficients for various β and KC , the experiments are carried out in several oscillation amplitudes and periods given in Table 5.

Table 5. Parameters used for the forced oscillation tests

Parameters	Symbol	Horizontal	Vertical
Mass of platform (kg)	M	42.2	42.2
Hydrostatic stiffness (N/m)	K_R	-	570.6
Oscillating amplitude (m)	a	0.1, 0.2	0.04, 0.08
KC number	KC	4.62, 9.24	0.9,1.8
Oscillating period (s)	T	1.6~3.0	1.6~3.0
Characteristic area (m^2)	A	0.3216	0.185
Displaced volume of water (m^3)	$\forall$	0.0422	0.0422

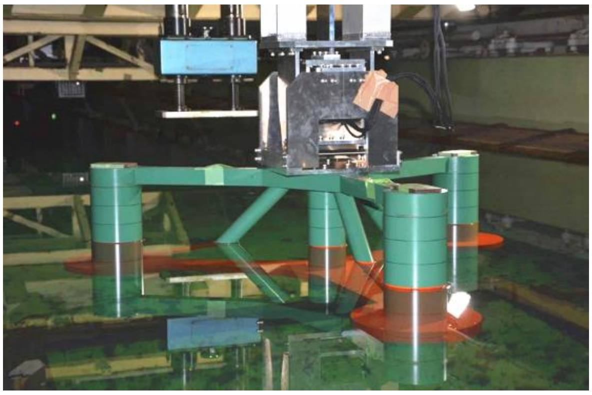

Figure 5. Forced oscillation test for a 1:50 scale model of semi-submersible platform

The global matrices of $[C_a]$ and $[C_d]$ of the model are described in Eq. (13). Diagonal terms of $[C_a]$ represent the added masses in the surge, sway and heave directions and the added moment of inertia in the roll, pitch and yaw directions. The off-diagonal terms denote the coupling between the motions in the relevant two degrees of freedom.

$$[C_a] = \begin{bmatrix} C_{a11} & 0.0 & 0.0 & 0.0 & C_{a15} & 0.0 \\ 0.0 & C_{a22} & 0.0 & C_{a24} & 0.0 & 0.0 \\ 0.0 & 0.0 & C_{a33} & 0.0 & 0.0 & 0.0 \\ 0.0 & C_{a42} & 0.0 & C_{a44} & 0.0 & 0.0 \\ C_{a51} & 0.0 & 0.0 & 0.0 & C_{a55} & 0.0 \\ 0.0 & 0.0 & 0.0 & 0.0 & 0.0 & C_{a66} \end{bmatrix} \quad [C_d] = \begin{bmatrix} C_{d11} & 0.0 & 0.0 & 0.0 & C_{d15} & 0.0 \\ 0.0 & C_{d22} & 0.0 & C_{d24} & 0.0 & 0.0 \\ 0.0 & 0.0 & C_{d33} & 0.0 & 0.0 & 0.0 \\ 0.0 & C_{d42} & 0.0 & C_{d44} & 0.0 & 0.0 \\ C_{d51} & 0.0 & 0.0 & 0.0 & C_{d55} & 0.0 \\ 0.0 & 0.0 & 0.0 & 0.0 & 0.0 & C_{d66} \end{bmatrix} \tag{13}$$

The non-zero terms in the global matrices can be calculated using the added mass and drag coefficients of each element as shown in Eqs. (14) and (15) [15].

$$\begin{aligned}
&C_{a11} = \frac{1}{\rho_w \forall} \sum_{i=1}^{N_W} \left[{}_iC_a^n \rho \forall_i^n \sin^2\theta_x + {}_iC_a^t \rho \forall_i^n \cos^2\theta_x \right]; \quad C_{a33} = \frac{1}{\rho_w \forall} \sum_{i=1}^{N_W} \left[{}_iC_a^t \rho \forall_i^n \cos^2\theta_z + {}_iC_a^n \rho \forall_i^n \sin^2\theta_z \right]; \\
&C_{a55} = \frac{1}{\rho_w \forall R^2} \sum_{i=1}^{N_W} \left[{}_iC_a^t \rho \forall_i^t \cos^2\theta_z \, x_i^2 + {}_iC_a^n \rho \forall_i^n \sin^2\theta_z \, x_i^2 + {}_iC_a^n \rho \forall_i^n \sin^2\theta_x (z_i - z_G)^2 + {}_iC_a^t \rho \forall_i^t \cos^2\theta_x (z_i - z_G)^2 \right]; \\
&C_{a66} = \frac{1}{\rho_w \forall R^2} \sum_{i=1}^{N_W} {}_iC_a^n \rho \forall_i^n \left[x_i^2 + y_i^2 \right]; \quad C_{a51} = \frac{1}{\rho_w \forall R} \sum_{i=1}^{N_W} \left[{}_iC_a^n \rho \forall_i^n \sin^2\theta_x (z_i - z_G) + {}_iC_a^t \rho \forall_i^t \cos^2\theta_x (z_i - z_G) \right]; \\
&C_{a22} = C_{a11}; \quad C_{a44} = C_{a55}; \\
&C_{a51} = C_{a15}; \quad C_{a24} = -C_{a15}; \quad C_{a42} = C_{a24}.
\end{aligned} \tag{14}$$

$$C_{d11} = \frac{1}{A_x}\sum_{i=1}^{N_w}\left[{}_iC_d^n A_i^n \sin^3\theta_x + {}_iC_d^t A_i^t \cos^3\theta_x \right]; \qquad C_{d33} = \frac{1}{A_z}\sum_{i=1}^{N_w}\left[{}_iC_d^t A_i^t \cos^3\theta_z + {}_iC_d^n A_i^n \sin^3\theta_z \right];$$

$$C_{d55} = \frac{1}{A_x R^3}\sum_{i=1}^{N_w}\left[{}_iC_d^t A_i^t \cos^3\theta_z |x_i|^3 + {}_iC_d^n A_i^n \sin^3\theta_z |x_i|^3 + {}_iC_d^n A_i^n \sin^3\theta_x |z_i - z_G|^3 + {}_iC_d^t A_i^t \cos^3\theta_z |z_i - z_G|^3 \right];$$

$$C_{d15} = \frac{1}{A_x R^2}\sum_{i=1}^{N_w}\left[{}_iC_d^n A_i^n \sin^3\theta_x |z_i - z_G|(z_i - z_G) + {}_iC_d^t A_i^t \cos^3\theta_x |z_i - z_G|(z_i - z_G) \right];$$

$$C_{d66} = \frac{1}{A_x R^3}\sum_{i=1}^{N_w} {}_iC_d^n A_i^n \left[\left(x_i^2 + y_i^2\right)^{3/2} \right];$$

$$\begin{aligned} &C_{d22} = C_{d11}; \quad C_{d44} = C_{d55}; \\ &C_{d51} = C_{d15}; \quad C_{d24} = -C_{d15}; \quad C_{d42} = C_{d24}. \end{aligned} \tag{15}$$

where θ_x and θ_z are the angles between the axial direction of cylinder and the global x and z axes respectively, N_w represents the number of element in water, z_G expresses the z-coordinate of center of gravity, x_i, y_i and z_i are the local coordinates of each element.

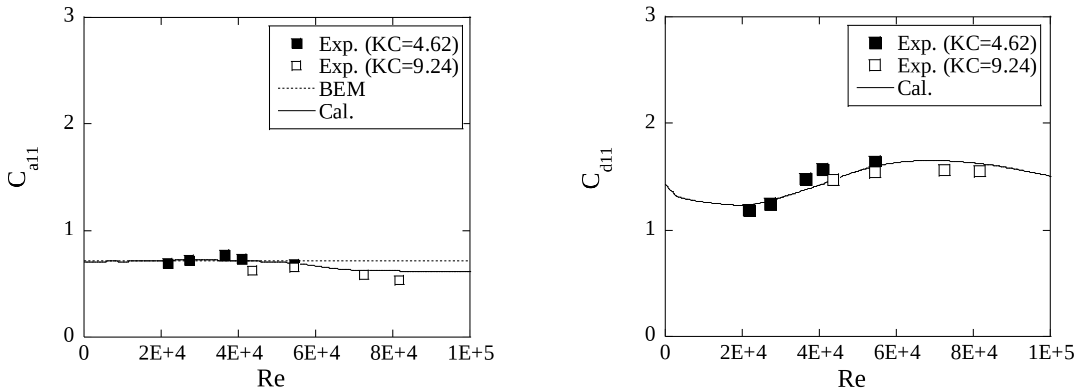

(a) Added mass coefficients in the surge direction (b) Drag coefficients in the surge direction

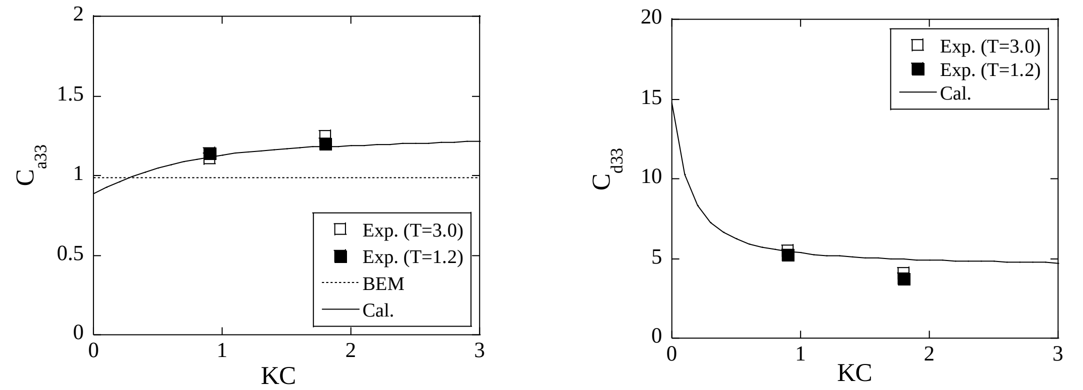

(c) Added mass coefficients in the heave direction (d) Drag coefficients in the heave direction

Figure 6. Global hydrodynamic coefficients of the scale model

The global hydrodynamic coefficients of the scale model are predicted by the proposed model and BEM. In Fig.6, the predicted global coefficients of C_a and C_d matches well with the experimental results under different Re and KC. The hydrodynamic coefficients in the surge direction change with Re, while the hydrodynamic coefficients in the heave direction show the variation with KC only. It is found that the alteration of C_a with Re in the surge direction is small, but the variation of C_d is obvious. The hydrodynamic coefficients in the heave direction are sensitive to KC due to the flow separation as shown in Zhang and Ishihara [11]. The predicted added mass coefficients of the platform in the surge direction by AQWA [20]shows small difference with those by the proposed model, while C_{a33} in the heave direction by AQWA is underestimated at large KC .

3.2. Dynamic response of the scale model in regular waves

The dynamic response of the scale model in regular waves is investigated by a water tank test. The rotor-nacelle-assembly (RNA) is modelled as a lumped mass and the hydrostatic characters of the scale model, such as gravity center and inertia moment, are adjusted by the distributed mass.

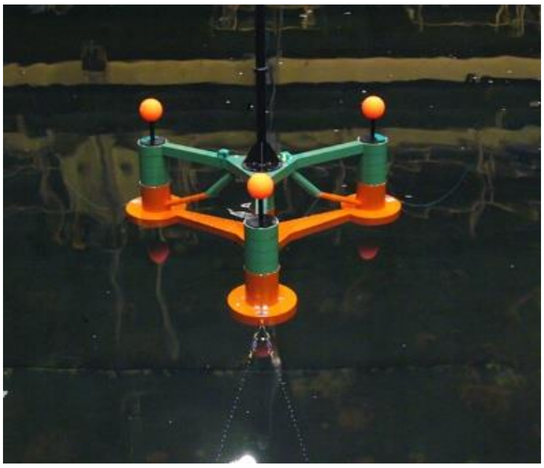

(a) Overview of the semi-submersible model in the water tank test

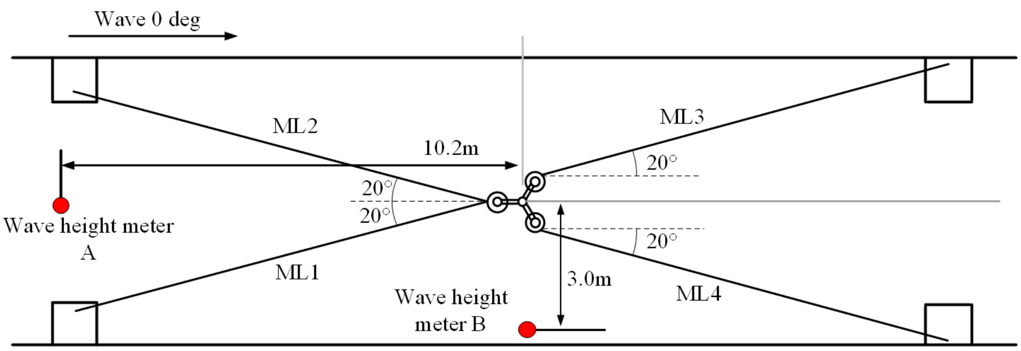

(b) Arrangement of mooring lines and sensors

Figure 7. Overview and configuration of the model used in the water tank test

Fig. 7 illustrates the configuration of the water tank test for dynamic response of the scale model. The model is positioned by 4 catenary mooring lines with a length of 10.353m anchored on the bottom of the water tank at a depth of 2.5 m. Two mooring lines on the left side are connected with Hp-1 and another two are connected with Hp-2 and Hp-3 respectively. The wave elevations during the experiment are recorded by two wave height meters installed in front of the wave generator and besides the model. The wave heights recorded by the meter A are used for simulations since the meter B is close to the wall of the tank and may be affected by the reflected wave. Three ball shaped passive reflectors are mounted on the top of side columns for recording the motion of the platform. Three cases of experiments are carried out as shown in Table 6. Case 1 and Case2 are conducted to confirm the initial tension of mooring lines and the natural periods of the model in the surge, heave and pitch directions. Dynamic response of the platform in regular waves with different wave heights are investigated in Case 3.

Table 6. Definition of the cases in the water tank test

Cases	Condition	Description
1	Still water	Static equilibrium test
2	Still water	Free decay test
3	Regular wave	H=0.02m, 0.10m; T=1.4~2.8s in model scale H=1m, 5m; T=9.9~19.8s in full scale

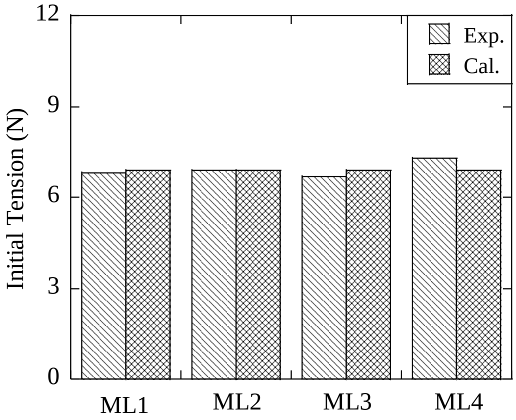

(a) Initial tension of mooring lines for the model

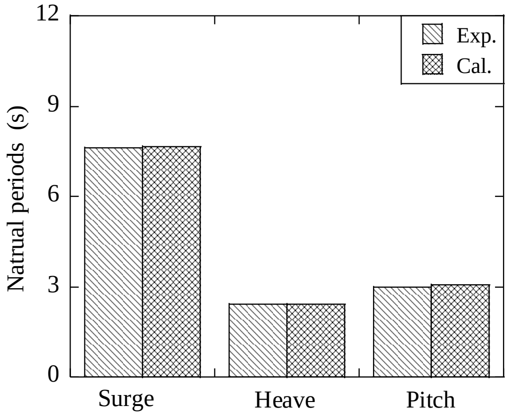

(b) Natural periods of the model

Figure 8. The predicted and measured initial tensions of mooring lines (Case 1) and natural periods of the model (Case 2)

The dynamic response of the motion and mooring tension in regular waves are evaluated by Orcaflex [21]. The hydrodynamic coefficients of each component are calculated by Eqs. (9) and (10). In each simulation, the global matrix of added mass is predicted by the proposed model instead of that obtained from BEM. The dynamic loading on the mooring lines are estimated by Morison's equation, where C_a and C_d in the normal direction are 1.0 and 1.8, respectively.

The predicted initial tensions of mooring lines and natural periods of the model show good agreement with the experimental data as illustrated in Fig. 8. The surge motions are almost linear since the natural period of surge is much longer than the peak wave period as shown in Fig. 9 (a). The response amplitude operator (RAO) of pitch in different wave heights show little difference when the wave period is large than 2s. The nonlinear drag force significantly contributes the response near the resonance range, which results in different RAOs under different wave heights as shown in Fig. 9 (b). The tension of mooring lines is nonlinear and increases as the wave height increases. The predicted RAOs show some discrepancies with the experimental data when the wave period is longer than 2.5s. It may be due to the limitation of wave generator since the wave height measured by the meter B is lower than that measured by the meter A when the wave period is longer than 2.5s, while this phenomenon does not be observed when the wave period is shorter than 2.5s.

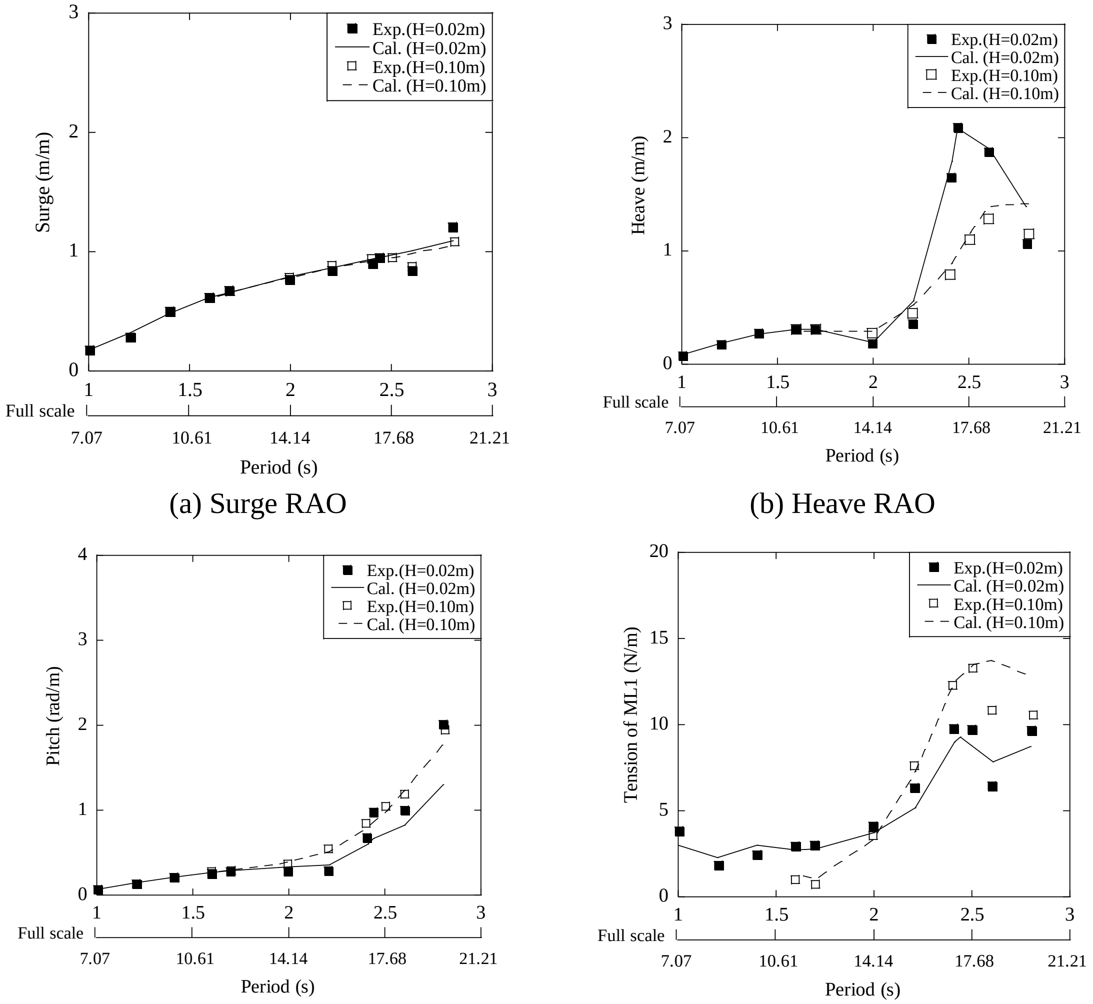

(a) Surge RAO (b) Heave RAO

(c) Pitch RAO (d) Tension RAO of ML1

Figure 9. The predicted and measured RAO of dynamic motion and tension in regular waves

3.3. Effect of skirts on dynamic response of the platform

A FOWT may experience resonant response when the natural period of motion is close to the peak wave period. The resonance increases the loading on the structure and affects the power production of wind turbine. The skirts installed on the bottom of the platform are generally applied to reduce the amplitude of motion.

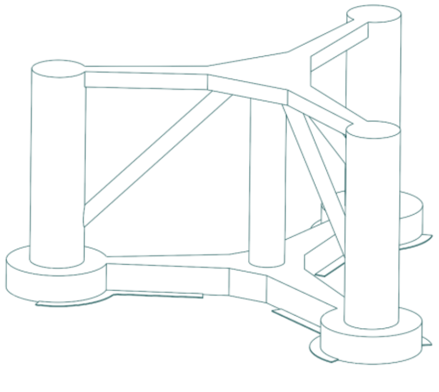

Figure 10. Overview of a semi-submersible platform with skirts

Table 7. Description of configuration for 1:50 and 1:60 scale models in full scale

	1:50 scale model	1:60 scale model
Displaced volume of water (m^3)	5275	4672
Draft (m)	19	16
Diameter of center column (m)	5	4.95
Diameter of side columns (m)	6.8	7.5
Center of gravity below SWL (m)	-8.3	-4.1
Radius of gyration Kxx (m)	20.5	22.2
Radius of gyration Kyy (m)	20.5	22.4
Water depth (m)	125	120

The viscous damping and added mass effects of the skirts are investigated based on a 1:60 scale semi-submersible model, in which the skirts are installed on the bottom of pontoons and heave plates as shown in Fig. 10. Table 7 describes the configuration of 1:50 and 1:60 scale models in detail.

The added mass of plate is dependent on the shape, such as circular or rectangular, while the drag coefficient significantly varies with the thickness of plates. A formula to predict C_a and C_d of plates with consideration of shape, thickness ratio and KC number effect are proposed by Zhang and Ishihara [11]. These formulas are modified and used to calculate the hydrodynamic coefficients of the skirts in the heave direction. The modification is conducted with consideration of the shape of skirt and its connection with pontoon and heave plates. The modified formulas are shown as:

$$C_a = k^3 - \frac{1}{4}[3r_d^2\sqrt{k^2 - r_d^2} + (k - \sqrt{k^2 - r_d^2})^2(2k + \sqrt{k^2 - r_d^2})] \tag{16}$$

$$k = k_1 \times k_2 \tag{17}$$

$$k_1 = 0.88 + 0.15KC \tag{18}$$

$$k_2 = \begin{cases} 1.00 & \text{Circular plate} \\ 0.95 & \text{Octgnonal plate} \\ 0.75 & \text{Square plate} \end{cases} \tag{19}$$

$$C_d = \min\left\{0.9r_t^{-1/3.7}(KC)^{-2.0/k_3}, 20\right\} \tag{20}$$

$$k_3 = \begin{cases} 2.5 & \text{Circular plate} \\ 2.5 & \text{Octgnonal plate} \\ 3.0 & \text{Square plate} \end{cases} \tag{21}$$

where k_1 represents the correction factor considering KC dependency for C_a. k_2 and k_3 account for the effect of geometry shape on C_a and C_d and the values corresponding to square plate are used for skirt. r_d is the ratio of diameter of attached column to that of the plate and it is defined as 0 since the skirts are very thin. r_t implies the ratio of thickness of skirt to its diameter or width. Since the flow fields near the edge of pontoons are changed due to the skirts, the interaction factors $\eta_a = 1.3$ and $\eta_d = 1.0$ for pontoon and heave plates in the normal direction is considered based on a numerical simulation by CFD.

The dynamic responses of motion and mooring tension of a 1:60 scale model without and with skirts are shown to in Fig. 11. The experimental data in Fig. 11 is obtained from the water tank test using a 1:60 scale model with skirts in the regular wave with the wave height of 0.05m. The

IOP Conf. Series: Journal of Physics: Conf. Series **1356** (2019) 012035 doi:10.1088/1742-6596/1356/1/012035

contribution of skirts on the surge motion is very limited because the hydrodynamic coefficients of the platform in the horizontal direction is unchanged. The heave and pitch motions of the model with skirts are smaller than those without skirts as shown in Fig. 11(b) and (c) since the skirts significantly increase viscous damping in the vertical direction. In addition, the natural period of heave for the model with skirts shifts to the long period since the added mass obviously increases with the skirts in the heave direction. The RAOs of the mooring tension of the model without and with skirt are close because the tension is mainly determined by the surge motion, which does not change. In the wave period from 2.2s to 2.7s, the RAO of the mooring tension for the platform with skirts is lower than that without skirts because of the lower heave motion of the model with skirts as shown in Fig. 11(d). This indicates that the installation of skirts is an effective method to avoid resonance of heave motion with waves and supress the vertical motion of platform.

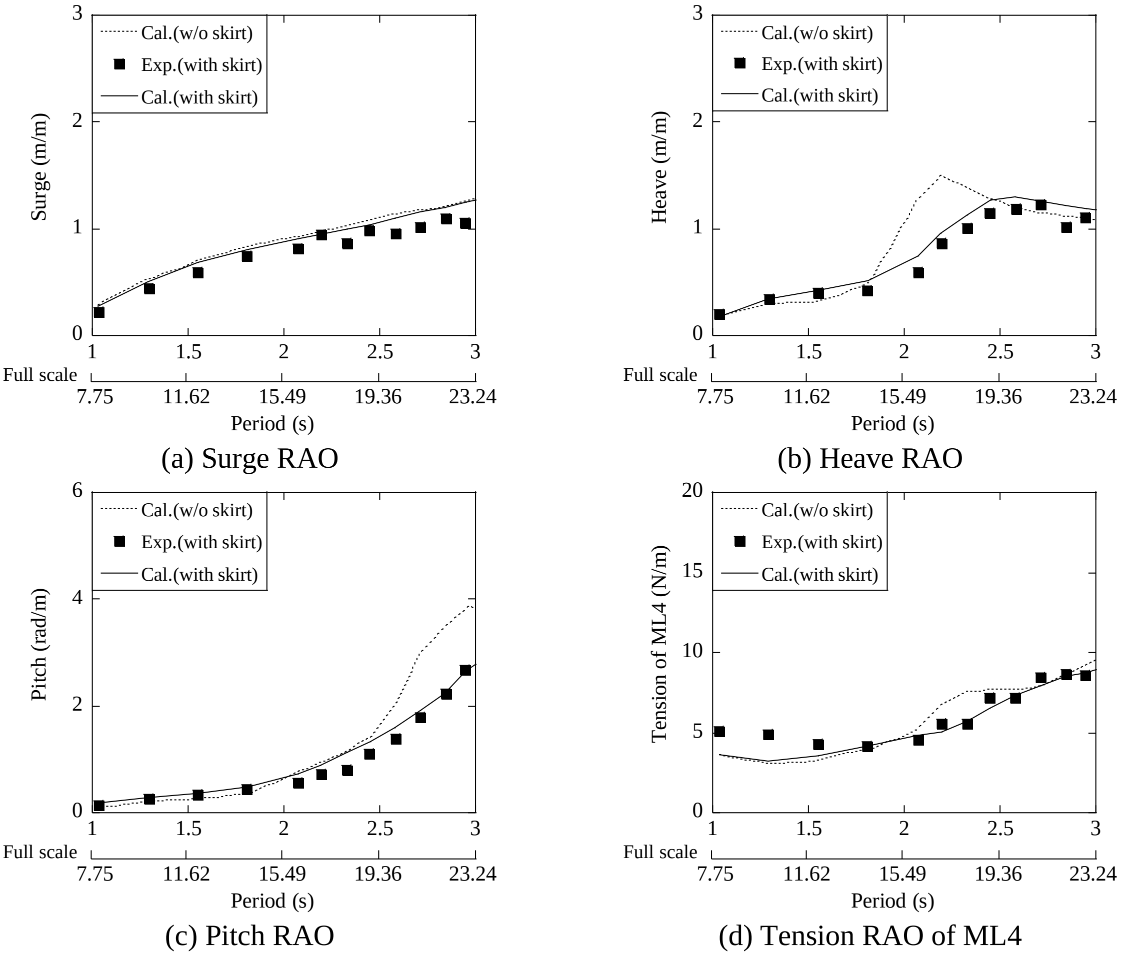

Figure 11. Predicted and measured RAO for the motion and mooring tension of a 1:60 scale model in regular waves

4. Conclusions

A novel hydrodynamic coefficient model for various components of FOWT is proposed. The predicted dynamic responses of the platform in regular waves are validated by the water tank tests. The conclusions are obtained as follows:

1. A novel hydrodynamic coefficient model for various components based on the water tank tests and numerical simulations is proposed to consider effects of interaction, frequency and amplitude on the hydrodynamic coefficients for various components of FOWT.
2. The predicted global matrices of hydrodynamic coefficients and dynamic response of FOWTs by the proposed model show good agreement with those obtained from the water tank tests.

3. The effect of skirts located on the bottom of platform is successfully simulated by the proposed hydrodynamic coefficient model. The increase of natural period and decrease of amplitude for the heave motion of FOWT can be explained by the increase of added mass and viscous damping in the vertical direction.

Acknowledgments
This research is carried out as a part of the Fukushima floating offshore wind farm demonstration project funded by the Ministry of Economy, Trade and Industry. The authors wish to express their deepest gratitude to the concerned parties for their assistance during this study.

Reference

[1] Hywind Demo: http://innovate.statoil.com/challenges/hywind/Pages/default.aspx
[2] Fukushima FORWARD: http://www.fukushima-forward.jp/english/index.html
[3] IDEOL's second demonstrator: https://www.ideol-offshore.com/en/japanese-demonstrator
[4] Faltinsen O. Sea loads on ships and offshore structures. *Cambridge university press*. 1993.
[5] DNV-RP-C205: Environmental conditions and environmental loads. *DNVGL*, Oslo, Norway, 2014.
[6] Benitz M A, Schmidt D P, Lackner M A, Stewart G M, Jonkman J, Robertson A. Validation of hydrodynamic load models using CFD for the OC4-DeepCwind semisubmersible. *In International Conference on Ocean, Offshore and Arctic Engineering 2015*, American Society of Mechanical Engineers. 2015.
[7] Robertson A, Jonkman J, Masciola M, Song H, Goupee A, Coulling A, Luan C. Definition of the semisubmersible floating system for phase II of OC4. *National Renewable Energy Laboratory*, 2014.
[8] Liang Y, Tao L. Interaction of vortex shedding processes on flow over a deep-draft semi-submersible. *Ocean Engineering*. 2017; 141:427-449.
[9] Wang X K, Tan S K. Flow around four circular cylinders in square configuration. *In 18th Australasian Fluid Mechanics Conference Launceston*, Australia. 2012.
[10] Sarpkaya T. In-line and transverse forces, On cylinders in oscillatory flow at high Reynolds numbers. *In Offshore Technology Conference*. 1976.
[11] Zhang S, Ishihara T. Numerical study of hydrodynamic coefficients of multiple heave plates by large eddy simulations with volume of fluid method. *Ocean Engineering*. 2018; 163:583-598.
[12] Lopez-Pavon C, Souto-Iglesias A. Hydrodynamic coefficients and pressure loads on heave plates for semi-submersible floating offshore wind turbines: A comparative analysis using large scale models. *Renewable Energy*. 2015; 81:864-881.
[13] Kamizawa K, Yoshimoto H, Awashima Y. The validation of the wave frequency motion of floating substation, *GRE2018*, Yokohama, Japan, 2018.
[14] Robertson A, Jonkman J, Vorpahl F, Popko W, Qvist J, Frøyd L, Chen X, Azcona J, Uzunoglu E, Soares CG, Luan C. Offshore code comparison collaboration continuation within IEA wind task 30: phase II results regarding a floating semisubmersible wind system. *International Conference on Ocean, Offshore and Arctic Engineering* 2014 American Society of Mechanical Engineers. 2014.
[15] Ishihara T, Zhang S. Prediction of dynamic response of semi-submersible floating offshore wind turbine using augmented Morison's equation with frequency dependent hydrodynamic coefficients. *Renewable Energy*. 2019; 131:1186-1207.
[16] Waris M B, Ishihara T. Dynamic response analysis of floating offshore wind turbine with different types of heave plates and mooring systems by using a fully nonlinear model. *Coupled systems mechanics*. 2012; 1(3):247-268.
[17] Pan J, Ishihara T. Numerical prediction of hydrodynamic coefficients for a semi-submersible platform by using large eddy simulation with volume of fluid method and Richardson extrapolation method. *EERA DeepWind'2019*, 2019.

[18] Tanaka N, Ikeda Y, Himeno Y, Fukutomi Y. Experimental study on hydrodynamic viscous force acting on oscillating bluff body. *Journal of the Society of Naval Architects of Japan*. 1991;169:85-92. (In Japanese)
[19] Tao L, Dray D. Hydrodynamic performance of solid and porous heave plates. *Ocean Engineering*. 2008; 35(10):1006-1014.
[20] AQWA: https://www.ansys.com/products/structures/ansys-aqwa
[21] OrcaFlex: https://www.orcina.com/SoftwareProducts/OrcaFlex/